Gasoline Fuels Properties for Multi-mode Operation – Observations in a GDI and the CFR engine

Ashish Shah, Alexander Hoth, Christopher P. Kolodziej, Toby Rockstroh

Argonne National Laboratory, 9700 S. Cass Avenue, Lemont, IL 60439, USA

1 Abstract

The combustion behavior of five full boiling range RON98 gasoline blends were evaluated for multi-mode operation in a GDI and the CFR octane rating engine. The GDI engine tests were conducted with stoichiometric air-fuel ratio in spark-ignition (SI), and with air-diluted homogeneous charge compression ignition (HCCI) mode. In the CFR engine, the knocking combustion was analyzed under standard RON testing conditions at both peak knocking lambda and stoichiometric air-fuel ratios, whereas compression ignited operation was characterized by utilizing the HCCI number test protocol. Disparate knock limited SI and

HCCI combustion behavior was observed for the test fuels, despite four of the fuels having the same RON and octane sensitivity. It was found that knock-limited combustion phasing in the GDI engine did not align well with the RON. However, a detailed comparison of knock-limited SI operation in the GDI and CFR engine revealed that a more appropriate effective RON based on a common knock intensity metric (MAPO) and stoichiometric air-fuel ratio resulted in comparable knock characterization between the two engine platforms. Furthermore, the critical intake air temperature and the critical compression ratio were proposed to characterize knock-limited SI operation, while the minimum intake air heating and compression ratio were used to define a fuel's autoignition propensity for compression ignition operation in the GDI and CFR engine, respectively. Finally, each fuel's characteristic compression ratio sweeps to obtain knock-limited SI (KLSI) and GCI operation was used to calculate an effective multi-mode octane number (MM-ON) based on the primary reference fuel blends.

Keywords: Octane sensitivity, Multi-mode Combustion

2 Introduction

The potential efficiency benefits of homogeneous charge compression ignition (HCCI) in four stroke gasoline engines were recognized more than three decades ago [1], [2]. However, it was also acknowledged that the operational limits of HCCI required switching to conventional gasoline engine operation to obtain high specific power output. This led to a

significant amount of research investigating lean part-load combustion strategies in multi-mode engines [3]–[5]. Concurrently, partially premixed combustion (PPC) with varying levels of stratification have been investigated to try and bring full time gasoline compression ignition (GCI) engines closer to market implementation [6]–[8]. Spark assisted compression ignition (SACI) or "mixed-mode" combustion has been shown to enhance combustion control and expand the operating range of HCCI [9]–[12]. Multi-mode combustion has garnered renewed interest of late with one vehicle OEM (Mazda) having started production of a multi-mode engine in early 2019 [13]. Apart from SACI, several other combustion control strategies have been implemented to enable multi-mode operation. For HCCI operation the temperature at the end of compression needs to be high enough to initiate auto-ignition while the high load SI operation will be constrained by the onset of knock. A trade-off therefore exists between compression ratio, intake air heating and/or use of retained exhaust gas residuals to enable multi-mode operation as well as combustion mode switching.

Similarly, the gasoline fuel for a multi-mode engine needs to fulfill two seemingly contradicting requirements. For HCCI operation at low load a fuel with a high auto-ignition propensity is desired, while the high-load SI operation demands a fuel with high knock resistance. Historically, gasoline knock resistance (or conversely, auto-ignition propensity) has been described by the research octane number (RON) and the motor octane number (MON) [14], [15]. It has since been shown that octane

number does not adequately describe knock resistance in modern SI engines. However, the octane index has been implemented as a practical means to utilize RON and MON as well as engine operating parameters to define a more accurate definition of the “octane appetite” in both modern SI and HCCI engines [16]–[20]. The applicability of the octane index rests on the premise that the cylinder conditions of the compressed gas mixture can be related to those attained during the RON or MON test. Modern charge boosted SI engines operate at compressed pressures that are higher than those obtained in the CFR engine under RON conditions. At the same time, intercooling of the intake charge reduces the temperature and therefore results in engine operation “beyond RON” [21]–[23]. Conversely, HCCI engine operation requires high compressed gas temperatures which generally push the operating range into the MON or “beyond MON” region [23]. It has therefore been argued that fuel octane sensitivity (RON-MON) could play a critical role in characterizing a fuel performance for a multi-mode engine [16].

The stochastic nature of knocking combustion in conventional SI engines is well documented [24]–[27], and has been described to follow a cyclically independent random process [28]–[30]. Knocking operation in the CFR engine under standard octane rating conditions has conversely been shown to be very repeatable, practically occurring during each combustion cycle and resulting with a distinct burn rate profile not akin to that observed in modern SI engines [31]–[37].

The variable compression ratio mechanism of the CFR octane rating engine has also been leveraged to study compression ignition behavior of gasoline like fuels. This has been done to study low temperature chemistry and HCCI fuel rating metrics [38]–[42].

The aim of this study is to evaluate the suitability of gasoline fuels with high RON and octane sensitivity towards enabling multi-mode operation in a modern GDI engine. For this purpose, five full boiling range gasolines with a RON of 98 were investigated. One of the test fuels had a low octane sensitivity of around 3 while the remaining fuels had a high sensitivity of around 10, albeit utilizing different chemical classes to generate the octane sensitivity. A detailed comparison of the combustion behavior under knock limited spark advance (KLSA) operation in the GDI and RON rating conditions in the CFR engine was conducted. Furthermore, autoignition properties of the fuel blends under HCCI combustion were characterized in the CFR engine and the GDI engine.

3 Apparatus and method

3.1 Experimental Facility

The experimental data used for this study was generated using a single cylinder gasoline direct injection (GDI) engine and a well-instrumented Cooperative Fuel Research (CFR) F1/F2 octane rating engine at Argonne National Laboratory (ANL). A brief description of these devices relevant to the present investigation is provided here, and the reader is referred

to previous publications [34], [43], [44] for more details about the experimental facility and their respective operating procedure.

3.1.1 Gasoline direct injection (GDI) engine

The setup consists of a prototype single-cylinder variant of a state-of-the-art multi-cylinder light duty gasoline direct injection engine, coupled to an AC dynamometer to dissipate power at required engine speed. Pertinent engine specification can be found in Table 1.

Intake air was supplied by an Atlas Copco compressor and throttling was achieved by using a pressure regulator upstream of the intake surge tank. A close coupled Osram-Sylvania SureHeat-MAX 6kW electric heater was used to maintain the desired intake air temperature. Gasoline fuel was supplied to the DI injector at a constant pressure of 150 bar by a stand-alone high-pressure fuel delivery system. Air and fuel flow rates were measured by Micro-motion Coriolis flow meters, and an AVL i60 integrated five-gas analyzer emissions bench was used to measure exhaust gas composition and thereby calculate engine's operating equivalence ratio.

Crank angle resolved indicated data was recorded using an AVL 620 Indimodule coupled to an AVL 365X crank angle encoder delivering 0.1 CAD resolution. Cylinder pressure was measured with a Kistler 6125C piezoelectric pressure transducer, and the intake and exhaust manifold pressures were measured by Kulite ETL-184A-190M and EWCTV-312(M) piezo-resistive pressure transducer, respectively. Other auxiliary

processes' pressures and temperatures, such as coolant temperature, were measured by general purpose pressure transducers and thermocouples through an in-house LabVIEW based data acquisition system at 1Hz sampling rate. All measurement devices were in calibrated state as per their respective manufacturer's recommendation at the time of use.

3.1.2 Cooperative Fuel Research (CFR) engine

In this work, the standard octane rating engine was equipped with state of the art instrumentation without affecting the engine's compliance with the ASTM D2699 RON method, as described in previous publications by the authors [34], [44]. The standard engine geometry is provided in Table 1. In addition to the ASTM knock-meter, the engine was also equipped with an AVL GU13Z-24 spark plug pressure transducer to allow for the simultaneous detection of high frequency pressure oscillations during knocking combustion. While the accuracy limitations of spark plug pressure transducers are well established, a previous study by the authors showed good correlation to a Kistler 6045 AU20 transducer flush mounted in the knock meter port under RON test conditions [45]. A wideband lambda sensor was used to enable accurate control for engine operation over a range of air-to-fuel ratios.

Table 1: Engine Specification

Parameter	**GDI Engine**	**CFR Engine**

Combustion Chamber	4-valve, 40° pent-roof	2-valve, pancake
Bore x Stroke [mm]	89.04 x 100.6	82.55 x 114.3
Connecting Rod [mm]	166.44	254
Displacement [L]	0.63	0.61
Compression Ratio [-]	12.6:1 & 15.3:1	Adjustable 4:1 - 18:1
Valve timings [aTDCf] Intake open/close Exhaust open/close	 -378 / -140 145 / 367	 -378 / -140 145 / 367
Fuel delivery	DI, 6-hole, solenoid	Carbureted
Ignition System	Inductive discharge	Capacitive discharge

156

157 3.2 Test Fuels

158 In order to better understand the impact of chemical compositional
159 variety on multi-mode engine combustion, the Co-Optima core research
160 gasolines designed as part of the Co-Optima Initiative [46] were utilized
161 for this study. Although the major chemical compositional classes of each
162 gasoline is diverse, all fuels were formulated to achieve similar research
163 octane numbers (RON), which facilitate investigation of chemistry
164 interactions that may differently respond to the auto-ignition

characteristic under knock-limited SI and compression ignited engine conditions. The key properties of the fuels are shown in Table 2, with the detailed chemical compositions and distillation properties given in the Appendix A. The Alkylate (ALK) fuel consists mostly of saturates resulting in near-zero octane sensitivity (i.e., the difference between RON and MON). The remaining four fuels contain approximately 30 volume percent of major classes - Ethanol (Oxygenates), Aromatics, Olefin and Naphthenic - identified by E30, A30, O30 and N30, respectively. This formulation leads to high octane sensitivity, but substantially different fuel autoignition chemistry.

Table 2: Fuel properties

Property	**Method**	**ALK**	**E30**	**A30**	**O30**	**N30**
RON (R)	D2699	98.0	97.4	98.1	98.2	98.0
MON (M)	D2700	96.6	86.6	87.8	88.0	87.1
S[a]	R - M	1.4	10.8	10.3	10.2	10.9
HoV[b]		309	565	412	337	393
PKL[c]		0.89	0.97	0.97	0.92	0.97

[a]S = Octane sensitivity

[b]HoV = Heat of vaporization [kJ/kg]

[c]PKL = Peak knock lambda at RON test conditions

3.3 Chemical Kinetic Calculations

The static auto-ignition characteristics of the fuels were used to aid pressure-temperature analysis of the cylinder charge under knock-

limited SI and compression ignited operation. For this purpose, isopleths of static auto-ignition delay were derived by performing constant-volume calculations using an advanced kinetic solver, Zero-RK [47] for a pressure range of 5-80 bar in steps of 5 bar, and 600-1200 K in steps of 20K, for stoichiometric as well as lean conditions relevant to HCCI operation. The latest version of a detailed kinetic mechanism for transportation fuels developed by Lawrence Livermore National Laboratory [48] was used. In this model, the core chemistry sub-model, C0–C4, is replaced with the recent Aramco 2.0 mechanism developed by NUI Galway [49], with updated sub-models for alkanes C5–C7 [50]–[52], iso-alkane [53], [54], aromatic compounds [55]–[57] cyclopentane chemistry [58]–[60], and EtOH chemistry [61]. It has been shown that trace amounts of NO can have a significant influence on auto-ignition chemistry [62]–[66]. In order to access the effect of NO under conditions relevant to this study, additional static auto-ignition delay calculations were performed, for which, the initial mixture included residual mass fraction determined by the Fox model [67]. For each fuel, the measured concentration of NO was used, while all other incomplete combustion products (UHC, CO) were excluded. The remaining residual mass was prescribed to be a mixture of complete combustion products (CO_2, H_2O and N_2), coming from a stoichiometric combustion, determined individually for each fuel according to the following formulae.

$$CH_\alpha O_\beta + \left(1 + \frac{\alpha}{4} - \frac{\beta}{2}\right)(O_2 + 3.773N_2)$$

$$= CO_2 + \frac{\alpha}{2}H_2O + \left(1 + \frac{\alpha}{4} - \frac{\beta}{2}\right)3.773N_2$$

where $\alpha = Molar\frac{H}{C}ratio, \beta = Molar\frac{O}{C}ratio$

Mole fraction for complete combustion:

$$CO_2 = \frac{1}{4.773 + 1.44325\alpha - 1.8865\beta}$$

$$H_2O = \frac{\alpha/2}{4.773 + 1.44325\alpha - 1.8865\beta}$$

$$N_2 = \frac{3.773\left(1 + \frac{\alpha}{4} - \frac{\beta}{2}\right)}{4.773 + 1.44325\alpha - 1.8865\beta}$$

The effect of NO was only estimated for stoichiometric conditions.

3.4 Experimental procedure

3.4.1 Gasoline direct injection (GDI) engine

Since the engine is not equipped with variable valve timing, a geometric compression ratio of 12.6:1 was used for SI mode and 15.3:1 was implemented for HCCI. After engine warm-up, the engine was run in SI mode at 1500 rpm, with a stoichiometric air-fuel ratio and 9 bar IMEP load. This operating condition was chosen in collaboration with industry partners as a representative knock-limited operating point for a SI engine at the chosen compression ratio of 12.6:1. In addition, this load also closely resembles the operating load of the CFR engine during standard RON tests, which was useful for the fuel performance comparison presented in this article. However, due to this similarity, it should be

noted that the analysis provided in this article mainly relates to naturally aspirated SI engine operating at full load, rather than knock limited operation in a highly boosted SI engines.The combustion phasing (crank angle at 50% mass fraction burnt – CA50%) was maintained at 20.5 degree after the firing top dead center (°aTDCf), while sweeping the intake air temperature from 35 – 75 °C or until a 300-cycle mean knock intensity, defined as maximum amplitude of pressure oscillation (MAPO), of 0.35 bar was reached.

For HCCI operation the intake air temperature and air-fuel ratio were adjusted until a combustion phasing of 12 °aTDCf and 3 bar IMEP was reached at 1500 rpm and intake air pressure maintained close to naturally aspirated at 1.05 bar absolute. The resulting excess air ratio (defined as actual air-fuel ratio divided by the stoichiometric air-fuel ratio, lambda, λ) was in the range of 3.35 – 3.85.

3.4.2 Co-operative Fuels Research (CFR) engine

The standard ASTM RON testing protocol was followed to characterize the RON ratings of the test fuels in the CFR engine [14]. This implied that each fuel was tested at 600 rpm and with a constant spark timing of -13 °aTDCf. While a typical RON test procedure would only require reporting the knock intensity at peak knocking lambda (PKL) operation, lambda sweeps were also conducted up to stoichiometry in this case. The compression ratio, spark timing, intake air pressure and intake air temperature upstream of the carburetor used during standardPKL

operation was kept constant throughout the lambda sweep and the change in knock intensity was recorded.

The HCCI fuel ratings were conducted according to the “MON-like” Lund-Chevron HCCI number test protocol [48] at 900 rpm. With a fixed intake temperature of 149 °C and excess air ratio of three (λ = 3.4), the compression ratio was adjusted for each fuel until stable combustion phasing (CA50) was obtained at 3 aTDCf.

4 Results and discussions

4.1 Multi-mode temperature delta

The applicability of RON and octane sensitivity towards describing the performance of the test fuels in the multi-mode engine was evaluated by correlating the RON and MON to the respective knock-limited SI and HCCI operation. Fuels with high RON and high-octane sensitivity (RON-MON) have previously been proposed as suitable for multi-mode SI-HCCI operation [16], [48].

In Figure 1 the knock-limited combustion phasing (KL-CA50) is shown as a function of RON. Recall that the knock limit was defined as 0.35 bar maximum amplitude of the pressure oscillations (MAPO), averaged over 200 consecutive cycles. Despite the fuels having a similar RON of 98, discernible differences in the knock-limited behavior of up to five crank angle degrees can be seen. The poor knock resistance of the ALK fuel with its low octane sensitivity agrees with the octane index framework.

However, although the remaining test fuels have a similarly high-octane sensitivity of around ten, significantly different knock-limited behavior was found.

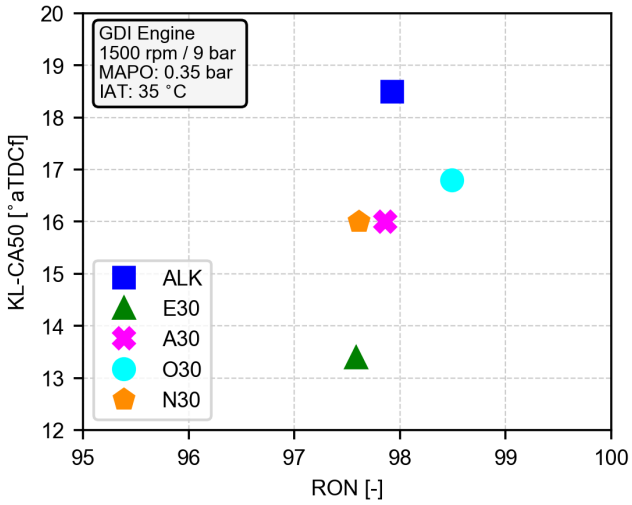

Figure 1 Knock-limited combustion phasing (KL-CA50) shown as a function of RON for the test fuels

This behavior was also replicated when analyzing the knock limited intake air temperature (KL-IAT), where a temperature difference of up to 40 °C was found between the test fuels, as shown in Figure 2. In this case the peak limited intake air temperature is depicted at a constant knock intensity of 0.35 bar (MAPO). For multi-mode engine operation fuels with a high KL-IAT need to be considered in order to enable knock-free SI operation at elevated compression ratios and high residual gas temperatures at intake valve closing during SI-HCCI transition.

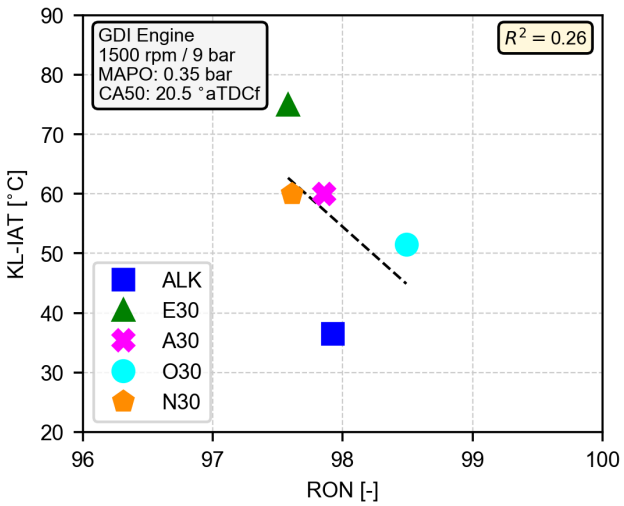

284 *Figure 2 Knock-limited (0.35 ± 0.1) intake air temperature (KL-IAT) shown as a*
285 *function of RON for the test fuels*

286 Under low load HCCI conditions the fuel's autoignition propensity can be
287 described by the intake air temperature requirement to obtain stable
288 combustion. The minimum intake air temperature for HCCI operation
289 (HCCI-IAT) is shown as a function of MON in Figure 3. The MON has been
290 suggested to be a more suitable method by which a fuel's performance
291 under HCCI operation could be characterized, and the intake
292 temperature conditions required for HCCI operation are relatively close
293 to the mixture temperature of 149 C prescribed in the MON test
294 protocol.. It is perhaps worth highlighting here that the MON method was
295 originally conceived to replicate the higher cylinder temperature
296 conditions prevalent in SI engines at the time [68]. While the ALK fuel
297 with the highest MON did require the highest amount of intake air
298 heating, discernible differences were noted among the remaining test
299 fuels, with A30 and O30 being distinct outliers. These observations are

echoed in a recent study by Szybist and Splitter who noted that highly aromatic gasoline blends required higher intake air temperatures for GCI operation, while olefinic blends were more reactive [69].

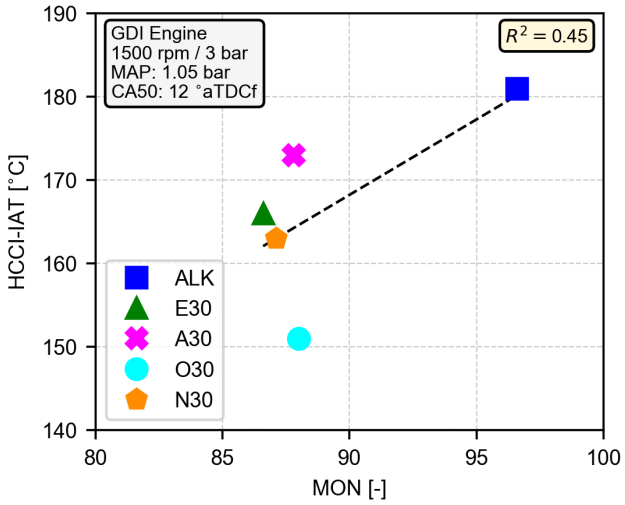

Figure 3 Minimum intake air temperature for HCCI operation (HCCI-IAT) shown as a function of MON for the test fuels

In order to enable knock-free SI operation at high load and stable HCCI combustion at low load, a fuel with somewhat contrasting autoignition characteristics is required. A “low temperature sensitivity” is desirable to prevent knocking operation under SI operation, while a “higher temperature sensitivity” under compression ignition operation would ease the transition to HCCI operation. This requirement can be replicated by the intake air temperature sweep shown in Figure 4, which is defined as the difference between the maximum knock limited intake air temperature and the minimum intake air temperature for HCCI operation. The ALK fuel was found to exhibit the highest intake

temperature sweep, needing the most intake air heating for HCCI operation and requiring the lowest air temperature at high load for knock limited SI operation. Although the remaining fuels have the same RON and octane sensitivity, discernible differences in the temperature dependencies for stable low load HCCI combustion and knock-limited high load SI combustion were found.

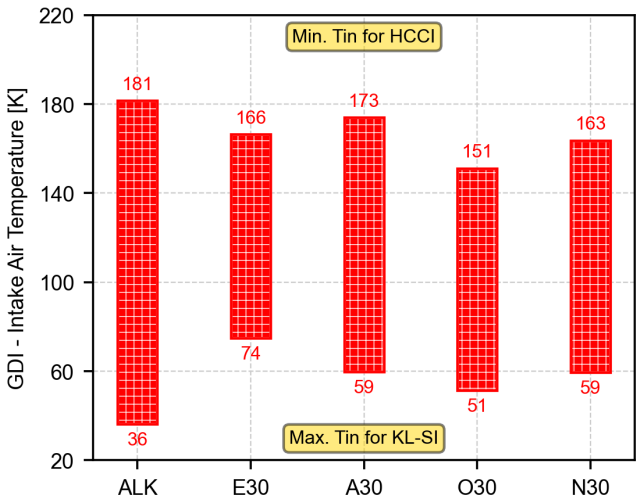

Figure 4: A bar plot showing intake air temperature change required for switch from knock-limited high load SI operation to low-load compression ignited operation

As noted earlier, octane sensitivity (RON – MON) at a fixed RON has been suggested to be a pragmatic method by which a fuel's performance in a multi-mode engine could be characterized. Following this argument, the octane sensitivity of the fuels was plotted against the intake temperature swing required on the multi-mode GDI engine (Multi-Mode ΔT) as shown in Figure 5. While a directional agreement with octane sensitivity could

be argued for the ALK and the remaining fuels, it should be noted that the temperature delta among the octane sensitive test fuels was found to be approximately 25 °C. Meanwhile, the temperature sensitivity between ALK and A30 was approximately 30 °C.

The intake air temperature for the RON test is controlled to approximately 52 °C and the mixture temperature for the MON test is approximately 149 °C. While the compressed temperature conditions characterize a fuel's temperature sensitivity to some degree, more complicated underlying autoignition properties of the fuels are at play, which are not captured by their octane numbers. In order to gain further insight, a detailed analysis of the SI and HCCI operation in the two engine platforms was conducted as will be discussed next.

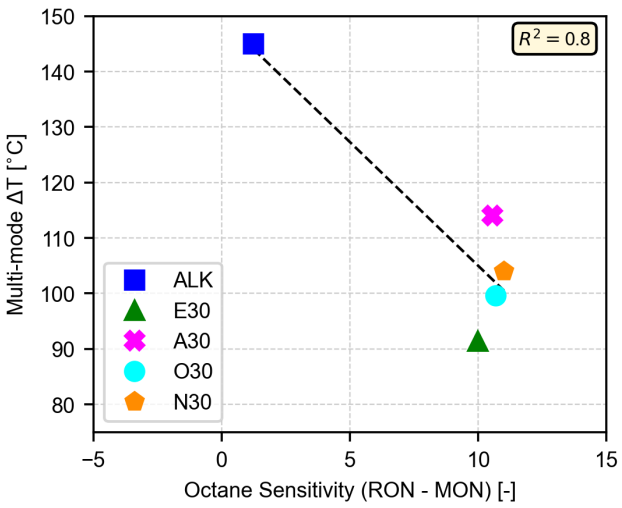

Figure 5: Plot showing correlation between octane sensitivity and Multi-mode ΔT_{in}.

4.2 Knock-limited SI operation

4.2.1 Intake temperature sweep in the GDI engine

The impact of intake air temperature on the knock intensity (MAPO) and the knock limited CA50 is shown in Figure 6. For the ALK fuel, the knock intensity limit of approximately 0.4 bar mean MAPO was reached at the lowest intake temperature of 35 °C, while E30 allowed for the intake temperature to be swept by a further 40 °C before the knock threshold was reached at 75 °C. The A30 and N30 fuels displayed similar behavior, while the O30 fuel was a bit more knock limited at elevated intake air temperatures. This ranking of the fuels' knocking behavior was also evident at 35 °C, where E30 depicted lowest knocking operation while some knocking cycles were detected for O30 and the knock threshold was reached for ALK. The cycle to cycle variation in knock intensity increased

for each of the fuels as the intake temperature was elevated, and the cyclic variability appears to be consistent among the fuels at their respective peak intake air temperatures. It is also worth highlighting that E30 appeared to provide a stronger knock resistance at elevated temperatures, which has previously been attributed to its higher HoV [70]. The knock limited combustion phasing CA50 behavior at a constant knock threshold of 0.35 bar followed the same trends for each of the test fuels. It is worth noting that the E30 fuel allowed for a significantly more optimal combustion phasing at 35 °C intake temperature, while this benefit started to diminish as the intake air was heated. However, at a fixed combustion phasing of around 19 aTDC, E30 allowed for significantly higher intake air heating than the remaining octane sensitive test fuels. Since the autoignition and knock propensity is dependent on the thermodynamic state of the gas at the end of compression, more insight may be gleaned from a cylinder pressure and temperature analysis that will be discussed later.

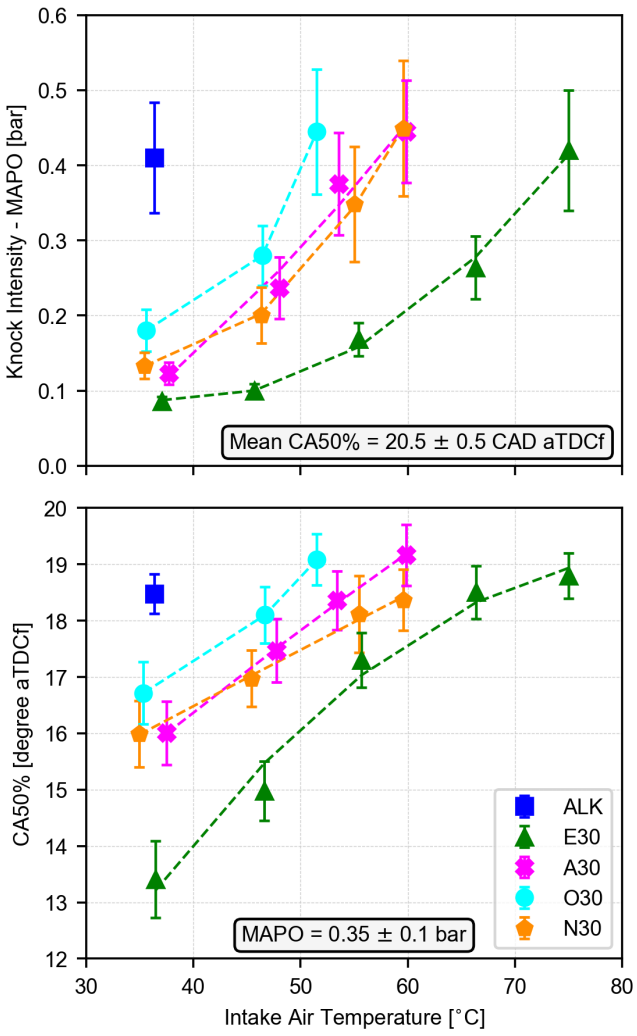

377 *Figure 6: Variation of a) knock intensity (mean MAPO) with intake air*
378 *temperature as fixed combustion phasing, and b) knock limited combustion*
379 *phasing with intake air temperature*

380 ### 4.2.2 Lambda effect on RON in the CFR engine

381 The RON test rates a fuel's octane number at "peak-knocking lambda"
382 (PKL), whereby the equivalence ratio is swept until the peak knock
383 intensity according to the ASTM knock-meter is found. For most fuels that
384 excess air ratio (Lambda) is slightly rich of stoichiometric in the region of

0.88 – 0.95. The respective PKL for the test fuels can be found in Table 2. A detailed discussion of the impact of the Lambda ratio on the knock-meter reading and knock intensity measured in terms of the maximum amplitude of pressure oscillations (MAPO) was presented by Hoth et al. [44]. These authors presented a method to provide corrected RON numbers based on the knock meter and MAPO reading at stoichiometric operation.

The RON values of the test fuels used in this study were re-calculated for stoichiometric operation in order to provide a more direct comparison to the knock limited SI operation in the GDI engine. The corrected numbers according to the method proposed by Hoth et al. [44] are shown in Figure 7, using both knock intensity (KI) interpolation and critical compression ratio (cCR) interpolation method. Regardless of the interpolation method, the effective stoichiometric RON of the ALK fuel reduces by more than one octane unit, while that of the sensitive fuels are relatively unchanged. The ALK fuel was also found to be most sensitive to the interpolation method, resulting in nearly one octane unit difference between KI-based and cCR-based rating method. In contrast, E30 was found to be insensitive to the interpolation method.

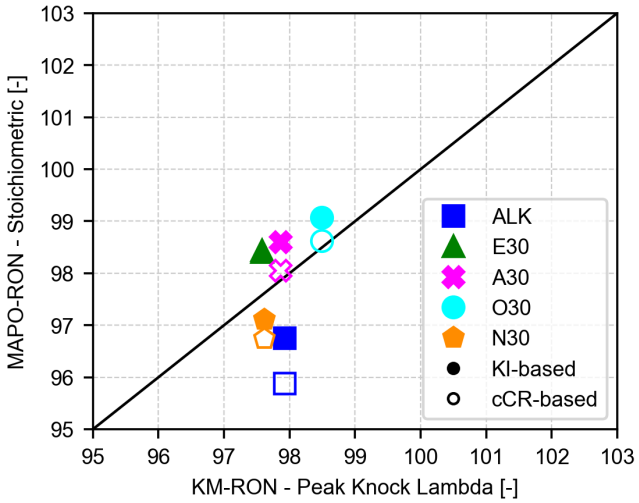

405 *Figure 7: Plot shows correlation between knock-meter based Octane rating at*
406 *peak knocking lambda ("Standard" RON) and MAPO-based Octane rating at*
407 *stoichiometric conditions on the CFR engine. Octane rating based on*
408 *interpolation on knock-intensity space (KI-based) at fixed compression ratio*
409 *("standard" method), and interpolation on critical compression ratio space (cCR-*
410 *based) at fixed knock intensity of 0.6 bar MAPO are shown.*

411 ### 4.2.3 Cyclic knock variability in the GDI and CFR engine

412 Knocking combustion in SI engines is well known to be a stochastic
413 process and this behavior is shown in Figure 15. It shows the bivariate
414 distribution of the knock intensity and combustion phasing. Referring to
415 the GDI engine data, the distribution of combustion phasing, at nominally
416 constant CA50 of 20.5 aTDCf is shown to be wide but normally
417 distributed. While a significant portion of the combustion cycles did not
418 display any knocking behavior, some cycles with extremely high knock
419 intensity constrained the knock limited combustion phasing (KLCA50).

The knock and combustion behavior of the CFR engine is shown to be significantly more repeatable, displaying a normally distributed behavior for both combustion phasing and knock intensity, under both PKL and stoichiometric operating conditions. The knock intensity was found to be similar between the two equivalence ratios, although a higher knock occurrence and subsequently earlier combustion phasing can be noted for the ALK fuel. For the remaining fuels, the equivalence ratio does not appear to affect the knock or CA50 phasing distribution, with the minor exception for the N30 fuel with an earlier combustion phasing. This analysis was extended by comparing the skewness and kurtosis of MAPO distributions for all operating conditions from the GDI engine (presented in Figure 6) to the operation in the CFR engine. Overall, the combustion phasing in the CFR engine is mostly defined by the fixed spark advance of 13 CA bTDC and the critical compression ratio defines the level of knock intensity. In the GDI engine the relatively high compression ratio of 12.6:1 necessitated a retarded KLSA resulting in a delayed combustion phasing.

4.2.4 Heat release behavior in the GDI and CFR engine

In order to analyze the combustion behavior in the two engine platforms, a heat release analysis was conducted, as shown in Figure 16. These plots show the most representative cycle determined by matching IMEP, CA50% and knock intensity of individual cycles with the sample mean, using weighing factors of 1, 2 and 4, respectively. As highlighted earlier, the start of combustion in the GDI engine can be seen to commence after the end of compression and burn late into the expansion phase. In the

CFR engine the combustion starts before TDC and centers around 10 aTDCf, leading to a higher rate of heat release than in the GDI engine. It should be noted that the rate of heat release was normalized here using totol cycle fuel energy,in order to remove the effect of fuel loading and engine speed. The heat release rate in the GDI engine was found to be consistent amongst the test fuels, except for the N30 fuel where a higher rate was found for the representative combustion cycle. In the CFR engine the equivalence ratio did not affect the heat release rate greatly, except for the ALK fuel which can be seen to have an earlier start of combustion, as previously highlighted in Figure 15. The circular marker on the cylinder pressure trace indicates the onset of knock. As highlighted in previous CFR engine studies, the so called “knock point” was defined as the inflection point in the cylinder pressure, where the onset of autoignition resulted in an increased burn rate [31], [37]. The knock point was subsequently shown to closely coincide with the onset of high frequency pressure fluctuations, indicative of knocking combustion. While the inflection point in the CFR engine pressure trace can be identified using a low pass filtered signal, the knock point inflection in the GDI engine is found more robustly by detecting the onset of high frequency pressure oscillation. Previous studies have highlighted that the knock point in the CFR engine can occur at burnt mass fractions of 50 – 80 %, depending on the compression ratio, i.e. octane rating of the fuel [31], [32]. In modern GDI engines, the quantity of the end-gas undergoing autoignition is generally only around 10 % .

To investigate this behavior, the normalized heat release rate is depicted as a function of mass fraction burnt, as shown in Figure 17. The onset of autoignition in the CFR engine can be clearly defined by the increase in the burn rate, which was found to occur around 60 – 70 % of the mass fraction burnt depending on the fuel. For the E30 and N30 fuel, the stoichiometric air-fuel mixture appeared to result in an earlier onset of autoignition, while the equivalence ratio did not play a role for the remaining fuels. It was notable that the onset of autoignition in the GDI engine also appeared to occur at a mass fraction burnt of around 70%, which could be due to the fact that the most representative cycle with higher-than-average knock intensity was plotted.

4.2.5 Thermodynamic state analysis at knock onset

In order to allow for a more thorough analysis of the thermodynamic state at the onset of autoignition in the two engine devices, compressed pressure and temperature maps were constructed as shown in Figure 18. For each of the fuels, the compressed temperature was estimated assuming isentropic compression. The gas temperature at intake valve closing was estimated using the empirical model of Fox et. al. [67]. In addition, an ignition delay contour map was created using constant volume chemical kinetic simulations, as described in section 3.3.. Nitrous oxide (NO) in the residual gas can have a profound impact on the autoignition behavior of the cylinder charge, as highlighted in recent RCM [71] and engine studies [62]–[64]. The ignition delay contours for a mixture including NO concentration from the residual gas fraction were

therefore included to study their impact on the ignition delay behavior, as described in section 3.3. A detailed investigation into the kinetic behavior of NO is beyond the scope of this study and will be addressed in a future publication. Furthermore, it should be noted that the impact of LTHR in the end gas is not considered using the isentropic compression analysis in this study. Recent studies have highlighted the impact of low and intermediate temperature chemistry in characterizing knock behavior [], especially under high load “beyond RON” operation. For the “near RON” operating conditions under consideration here the impact of preliminary was deemed to have less of an effect and was subsequently not included.

Starting with the ALK fuel in the top left, the observations of the fuels will be discussed in a clockwise manner in Figure 18. For the ALK fuel, one compression trajectory for the GDI engine is depicted since the knock limited intake temperature was constrained to 35 °C. The star marker indicates the ignition point at around 20 bar and 800 K, while the round markers show the location of CA10 followed by CA50. The start of autoignition is demarcated by the blue square marker for the case of the ALK fuel and lies approximately on the 2 ms ignition iso-tau contours. For the CFR engine, the black line depicts the stoichiometric operating case, while the grey trajectory shows the PKL case. The mixture is ignited at around 12 bar and 680 K, and the combustion midpoint roughly coincides with the CA10 marker of the GDI engine at around 30 bar and 850 K. For the stoichiometric case the start of autoignition occurs around 35 bar and

900 K, while the PKL occurs at a slightly higher pressure. Since the CFR engine is operating at less than half the speed of the GDI engine, the knock point correlates with the 4 ms ignition delay isopleth.

For the other fuels, the intake temperature sweep depicted in Figure 6 translates into different compression trajectories in the GDI engine. As the intake temperature was increased, the compressed temperature at the time of spark increased as well and could span a range of up to 100 K, in the case of E30. The onset of autoignition meanwhile appeared to occur at relatively similar temperatures, aligning approximately with the profile of the isopleth contours.

The impact of NO can be seen to be more pronounced in the negative temperature coefficient (NTC) region for each of the fuels. This suggests that NO could therefore have a profound impact on the knocking behavior in the CFR engine, since the compression trajectories traverse the NTC region and the onset of autoignition occurs at the cusp of this region before transitioning into the intermediate temperature regime. It should be noted that the effect of NO during standard RON conditions may differ due to operation with slightly rich air-fuel ratios, where both the static auto-ignition characteristics of the fuel and the effect of NO may be different.

In order to investigate the impact of rate of compression between the two engines, the pressure-temperature framework was expanded to include the time domain as shown in Figure 19. The compression

trajectories were depicted on a temperature-time and a pressure-time plane. The NTC temperature band is provided for guidance in order to discuss the potential impact of low-temperature chemistry during the compression process. The significantly longer duration of the compression process for the CFR engine is self-evident. However, it is interesting to note that the time spent in the temperature range above 700 K and up to the start of autoignition is similar in both engines. As highlighted in Figure 4, significant differences in the knock-limited intake temperatures were found amongst the fuels in the GDI engine, although this behavior was not replicated by the critical compression ratio in the CFR engine.

4.3 Low-load Compression Ignited Operation in the GDI and the CFR engine

Compression ignition operation in the GDI engine was achieved by intake air heating while the compression ratio was adjusted in the CFR engine. In both cases the compressed gas temperature was elevated until autoignition was achieved, as will be discussed in more detail here.

4.3.1 Thermodynamic state analysis at CA10

The compression trajectories for the compression ignited operation are shown in Figure 8. The compression histories for the GDI engine are again depicted in red, with the fuel specific marker indicating the start of combustion (CA10). Similarly, black trajectories are implemented for the CFR engine, with the fuel markers indicating the location of CA10. The

standard RON and MON trajectories are provided for reference. The ALK fuel required the highest compressed temperature of around 1150 K, while O30 ignited at around 1070 K in the GDI engine. The same order of reactivity amongst most of the test fuels was noted in the CFR engine, except for E30 which was found to be more reactive in the CFR engine than in the GDI engine. Since the CFR engine was operating at almost half the engine speed of the GDI engine, the start of combustion correlates with a constant ignition delay time of around 2 ms instead of 0.5 ms for the GDI engine case.

The effect of the compression time can be highlighted by again expanding the PT-framework into the time domain, as shown in Figure 9. Compared to the 600 rpm SI case highlighted in Figure 19, the compression times for the HCCI cases are closer to those in the GDI engine. The dashed line provides the approximate NTC region for the test fuels and indicates that the 'residence time' in this region is similar in both engine platforms.

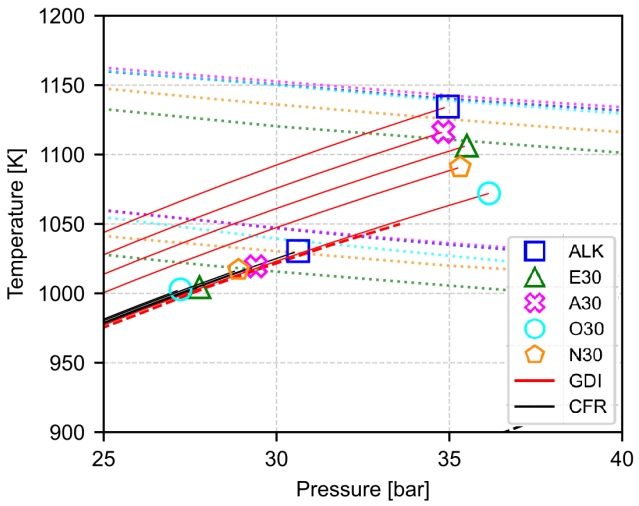

578 *Figure 8: HCCI PT trajectories with iso-tau lines (0.5 and 2 ms)*

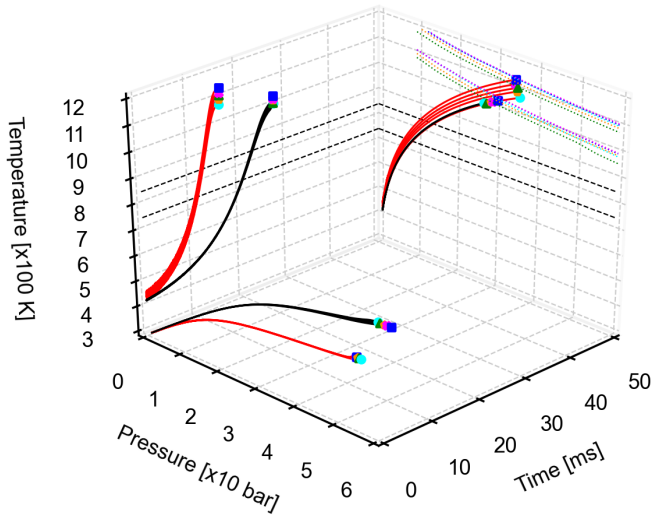

580 *Figure 9: HCCI P-T-time plot*

581 4.3.2 Heat release analysis in the GDI and CFR engine

582 Figure 20 shows representative cycles of the cylinder pressure and heat

583 release rates observed in both engine platforms for all of the test fuels.

584 In the GDI engine the earliest combustion phasing was limited to 12

585 °aTDC in order to avoid excessive combustion noise, while in the CFR

586 engine this phasing was controlled to 3 °aTDC with the aid of the
587 compression ratio, in line with the HCCI number (HCCI#) rating method
588 described previously [38], [72]. Although the equivalence ratio was fairly
589 similar between the two engine platforms, the peak rate of heat release
590 was significantly higher in the GDI engine than in the CFR. It should be
591 noted here that the heat release rate was again normalized in order to
592 remove differences due to fuel loading in the two platforms. It is worth
593 mentioning here that the turbulence intensity in the GDI engine is
594 expected to be significantly higher than in the CFR engine, due to the
595 higher engine speed and the intake ports that are designed to generate
596 tumble. Although the CFR engine is equipped with a swirl inducing
597 shrouded intake valve, the turbulence level are evidently lower than
598 those in the GDI engine.

While appreciable differences were noted in the intake air and compression ratio requirements for the different test fuels, the subsequent heat release behavior was found to be very comparable between the fuels. This behavior is also depicted in Figure 21, where the normalized heat release rate is plotted as a function of mass fraction burnt. Preliminary exothermicity was not noted during any of the tests.

4.4 Discussion

The deficiencies of the RON and MON method to characterize knock behavior for modern SI engines are well established. While the octane index provides a practical method to correct for the thermodynamic states in current engine designs, the method has its limitations and has been shown to not be entirely fuel independent [19], [75], [76]. Furthermore, the octane index metric has been shown to break down when trying to characterize autoignition quality properties for the use in gasoline compression ignition engines. Since the RON and MON number characterize a knock intensity rather than autoignition quality, this non-conformance may perhaps be expected. Of course, knock onset is inarguably linked to the onset of autoignition, however, the resulting knock intensity has been shown to be fuel dependent. Furthermore,

620 discrepancies between knock intensity and the knock-meter reading
621 during the standard octane test have also been highlighted.

622 The detailed combustion analysis of the RON98 fuels under SI and HCCI
623 operation further highlights the non-conformance of RON and octane
624 sensitivity towards characterizing fuel performance in a multi-mode
625 engine. This is replicated in Figure 10, where the intake air temperature
626 and compression ratio change are shown for the GDI and CFR engine,
627 respectively. When comparing the non-octane sensitive ALK fuel to the
628 remaining test fuels, the octane sensitivity provides a directional
629 indication of a fuel's knock resistance and autoignition propensity.
630 However, significant differences in the critical temperatures for SI and
631 HCCI operation in the GDI engine were found for four of the test fuels
632 having the same RON and octane sensitivity. Similar behavior was noted
633 when analyzing the critical compression ratio for the two combustion
634 modes in the CFR engine.

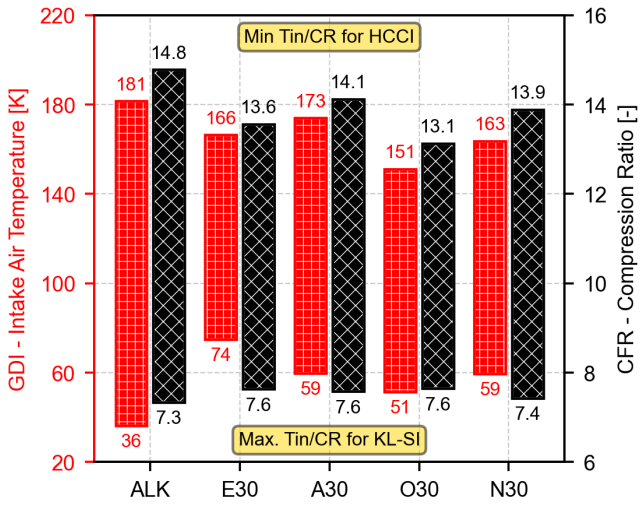

636 *Figure 10 A bar plot showing intake air temperature change or compression ratio*
637 *change required to switch from knock-limited SI operation to low-load*
638 *compression ignited operation in the GDI and CFR engine.*

639 One of the major differences between the CFR engine operating
640 conditions and those in conventional SI engines, is the effect of the
641 equivalence ratio on knocking behavior. The RON 98 fuels investigated in
642 this study had considerably different octane ratings when corrected for
643 stoichiometric operation, as was highlighted in 4.2.2. When correcting
644 the RON for stoichiometric operation and utilizing the MAPO knock
645 intensity metric, an improved fit with the KL-IAT was found, as shown in
646 Figure 11.

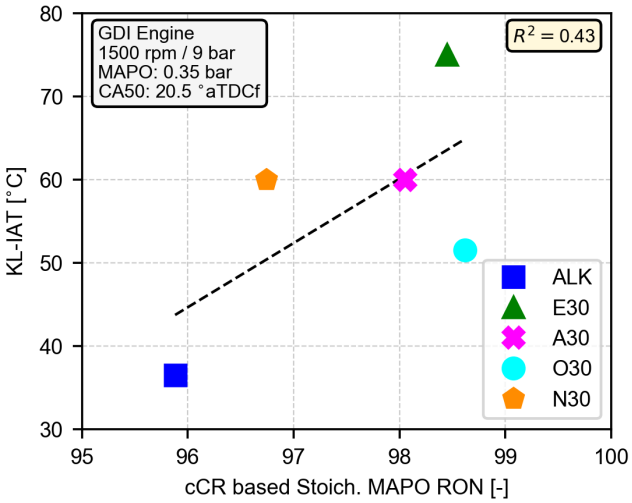

Figure 11 KL-IAT in the GDI engine as a function of Stoichiometric MAPO-based RON obtained from the CFR engine.

The variable compression ratio mechanism of the CFR engine also lends itself to characterize the autoignition quality in HCCI mode, as discussed in 4.3. In Figure 12 the minimum intake air temperature in the GDI engine is shown as a function of the HCCI#. A good correlation was found, implying that the ranking of autoignition propensity of the fuels is captured similarly in both engine platforms. This is also in agreement with the comparison of the minimum intake temperature and critical compression ratio in the two engine platforms, highlighted in Figure 10.

This GDI Multi-mode ΔT, as previously shown in Figure 5, is now shown in Figure 13 as a function of the Δ-cCR in the CFR engine. This resulted in a good correlation, indicating that the compression ratio metric captured the temperature sensitivities in the GDI engine under multi-mode operation. The critical compression ratio was then converted to an

663 effective ON (by interpolation critical compression ratio space for PRF
664 fuels) as shown in Figure 14, which further improved the correlation.

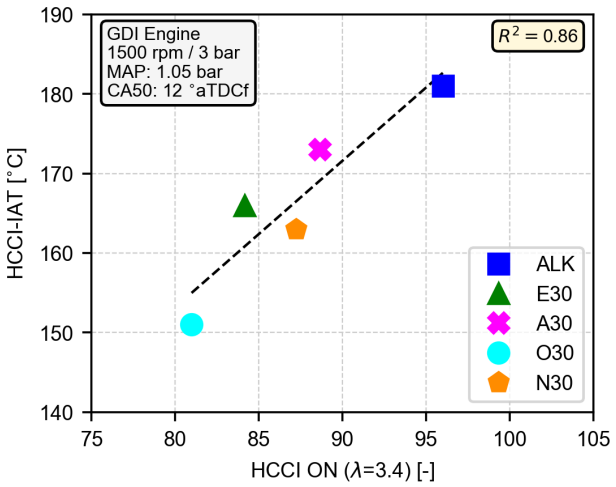

666 *Figure 12 Plot shows correlation between the HCCI ON (measured at 900 rpm, 1*

667 *bar, 150 °C, λ = 3.4 in the CFR engine) and the minimum intake air temperature*

668 *required for HCCI in the GDI engine*

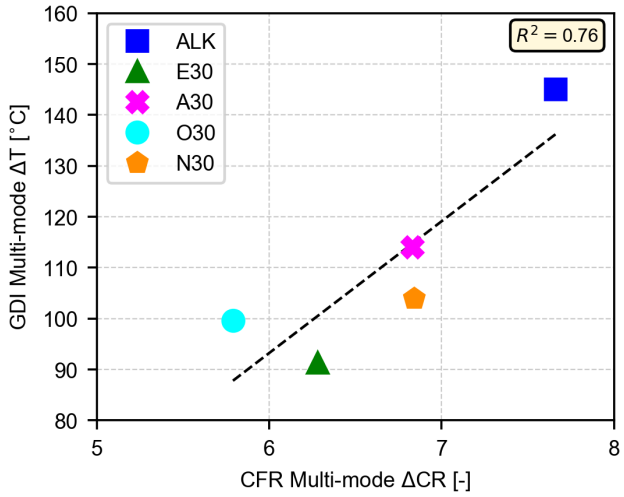

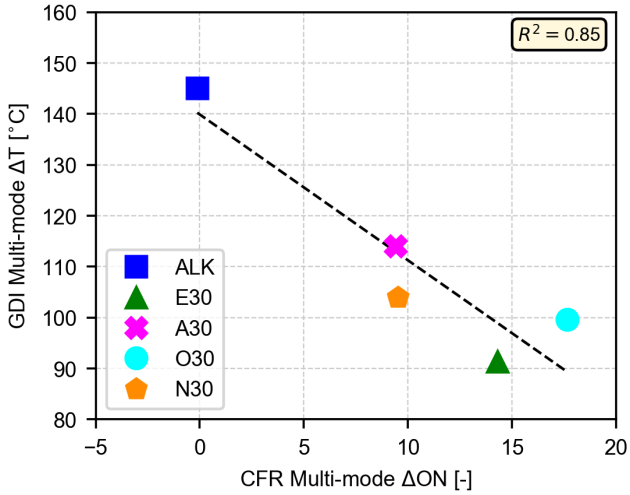

673 *Figure 14: Plot showing correlation between CFR engine-derived Δ-ON for multi-*
674 *mode operation, and ΔT_{in} for multi-mode operation on the GDI engine.*

675 5 Conclusion

676 A detailed analysis of the combustion behavior in the CFR engine and a
677 multi-mode GDI engine was conducted, and the following conclusions
678 can be drawn:

679 • Standard RON, MON and S are insufficient to describe autoignition
680 behavior in a multi-mode engine
681 • RON and MON describe a (low pass filtered) knock intensity which,
682 by its nature, appears to be insufficient to describe autoignition
683 characteristics under compression ignited operation.
684 • Correlation between KLSI and RON can be improved by correcting for
685 stoichiometry and knock intensity metric

- A critical compression ratio metric for SI and ACI operation on the CFR engine appears to show some promise in rating fuels for modern multi-mode engines

6 Acknowledgements

The submitted manuscript has been created in part by UChicago Argonne, LLC, Operator of Argonne National Laboratory ("Argonne"). Argonne, a U.S. Department of Energy Office of Science laboratory, is operated under Contract No. DE-AC02-06CH11357. Funding for this work was received from the Office of Vehicle Technology, Office of Energy Efficiency and Renewable Energy, U.S. Department of Energy, as part of the Co-Optimization of Fuels & Engines (Co-Optima) project. The authors would like to acknowledge the support of Lawrence Livermore National Laboratory for their support with the chemical kinetic mechanisms and Dr. Song Cheng for running the kinetic simulations using the Zero-RK toolset.

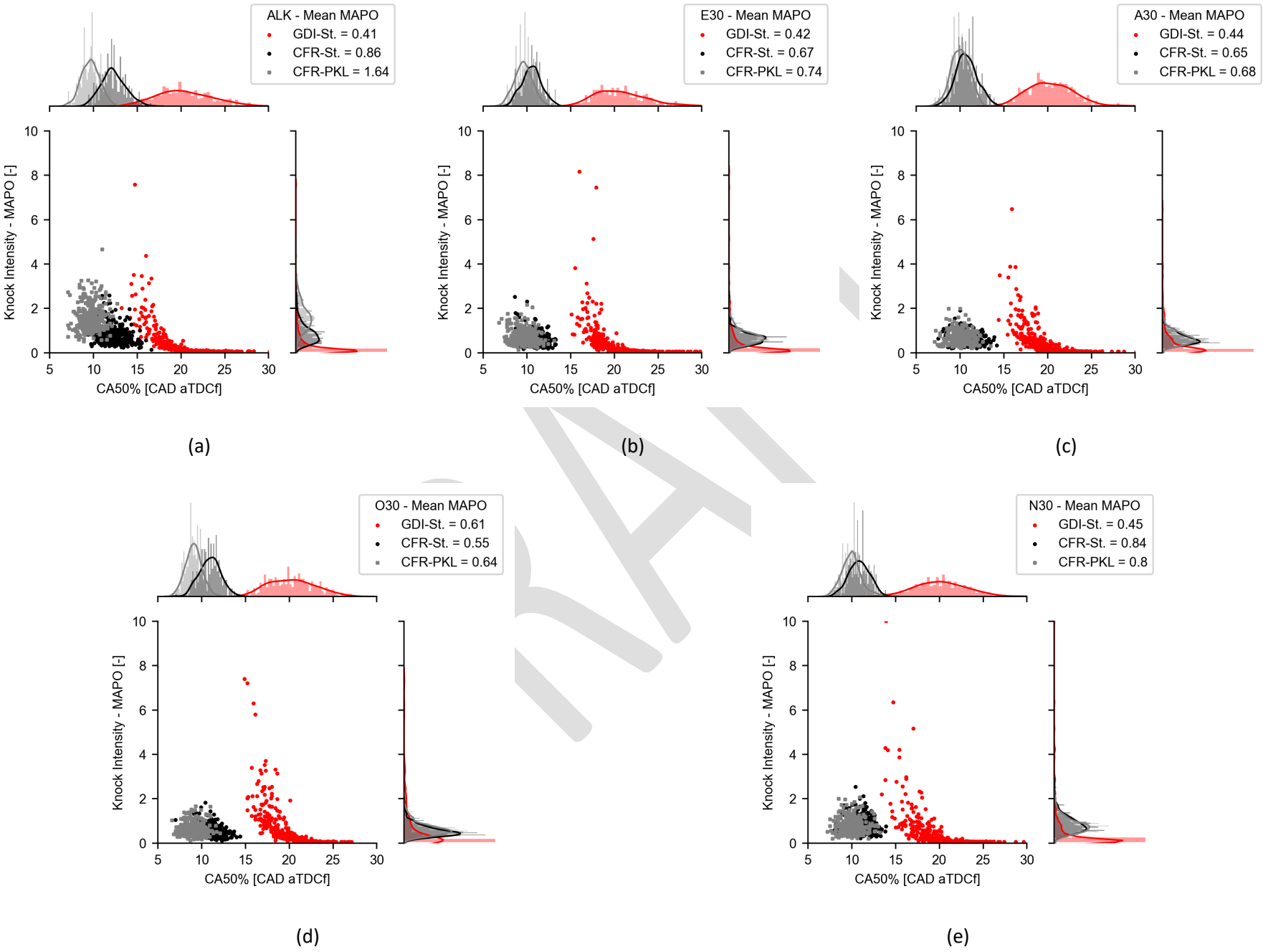
ALK - Mean MAPO
GDI-St. = 0.41
CFR-St. = 0.86
CFR-PKL = 1.64
E30 - Mean MAPO
GDI-St. = 0.42
CFR-St. = 0.67
CFR-PKL = 0.74
A30 - Mean MAPO
GDI-St. = 0.44
CFR-St. = 0.65
CFR-PKL = 0.68
O30 - Mean MAPO
GDI-St. = 0.61
CFR-St. = 0.55
CFR-PKL = 0.64
N30 - Mean MAPO
GDI-St. = 0.45
CFR-St. = 0.84
CFR-PKL = 0.8
Knock Intensity - MAPO [-]
CA50% [CAD aTDCf]
(a)
(b)
(c)
(d)
(e)

Figure 15: Bivariate distribution of combustion phasing (CA50%) and knock intensity (MAPO) for operation in the GDI engine at stoichiometric condition (red) and CFR engine at peak-knock-lambda (blue) and stoichiometric condition (orange)

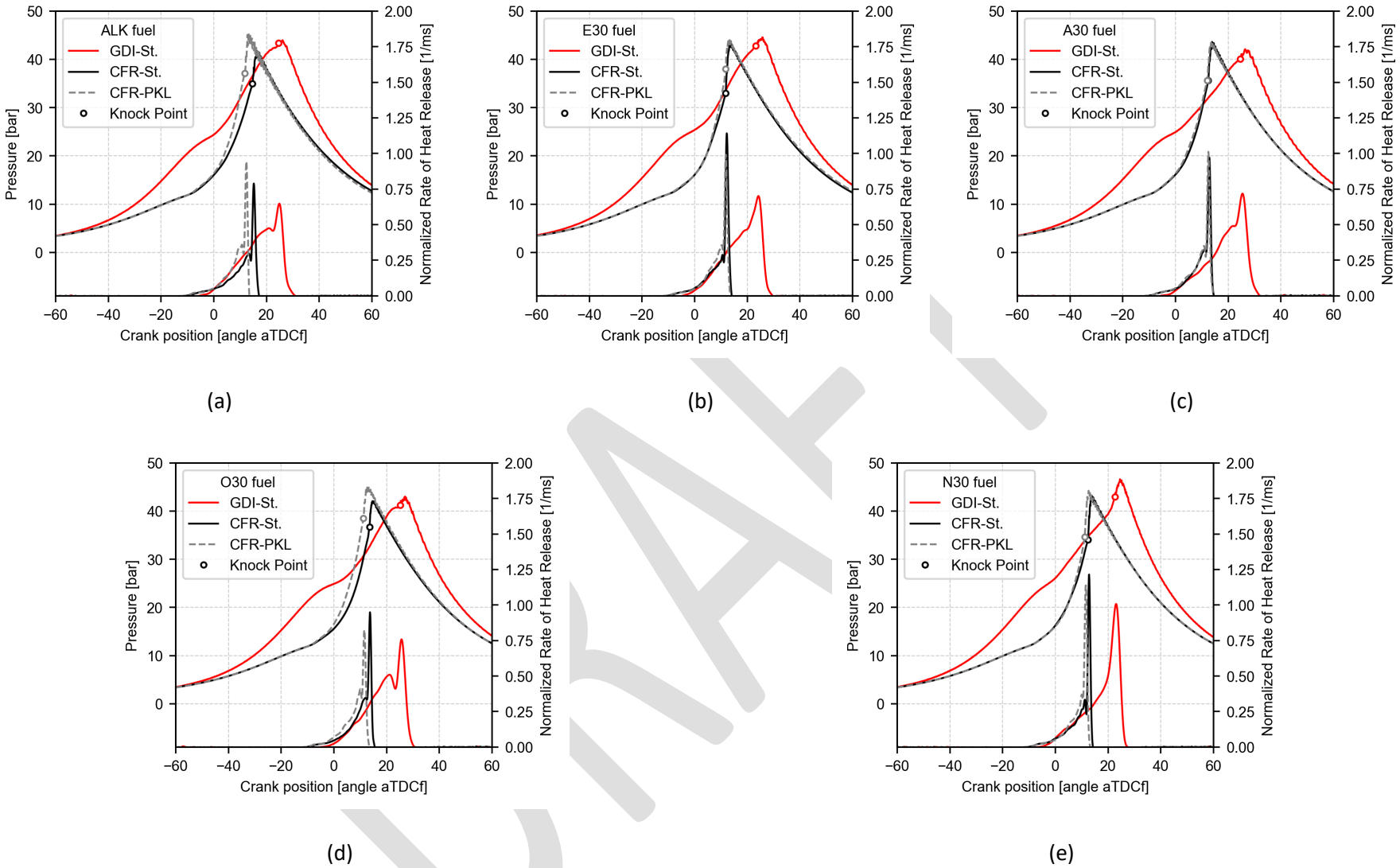

Figure 16: Cylinder pressure and heat release rate characteristics in the GDI engine at stoichiometric condition (red) and CFR engine at peak-knock-lambda (blue) and stoichiometric condition (orange)

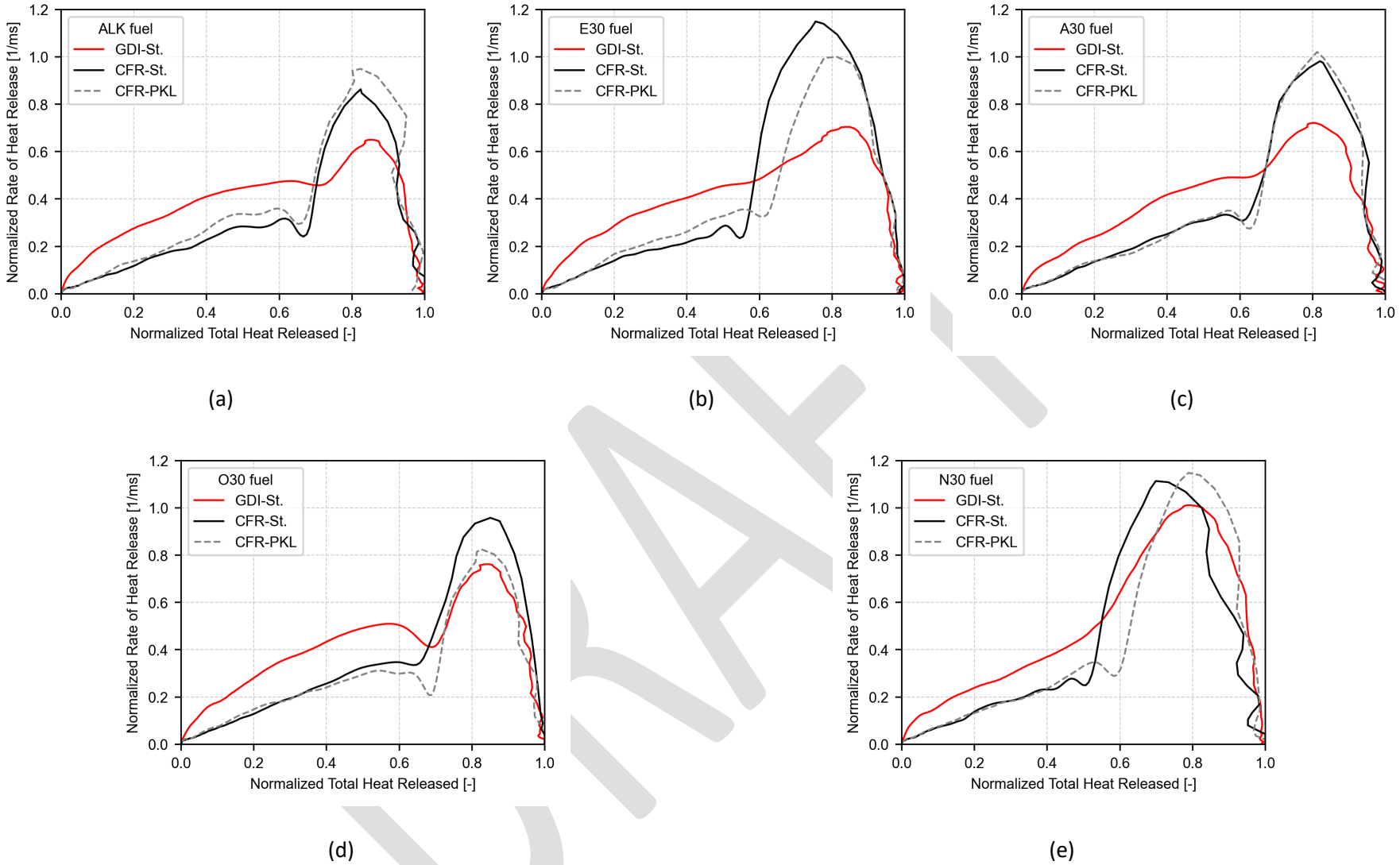

Figure 17: Normalized heat release rate plotted against normalized total heat released for operation in the GDI engine at stoichiometric condition (red) and CFR engine at peak-knock-lambda (blue) and stoichiometric condition (orange)

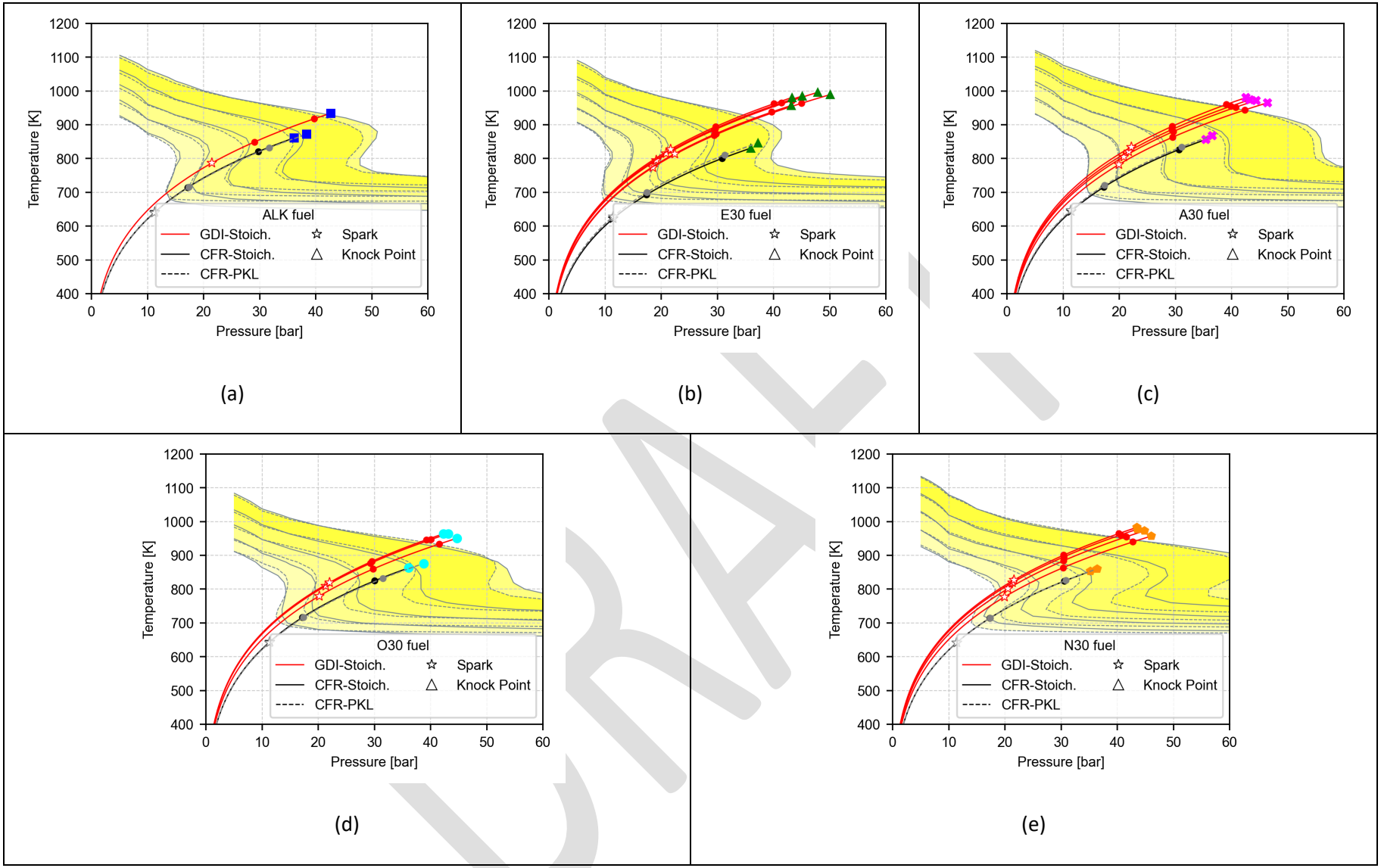

Figure 18: KL-SI PT trajectories with iso-tau lines (2, 4, 8, 16, 32 ms). Solid lines is without NO, dashed line is with NO.

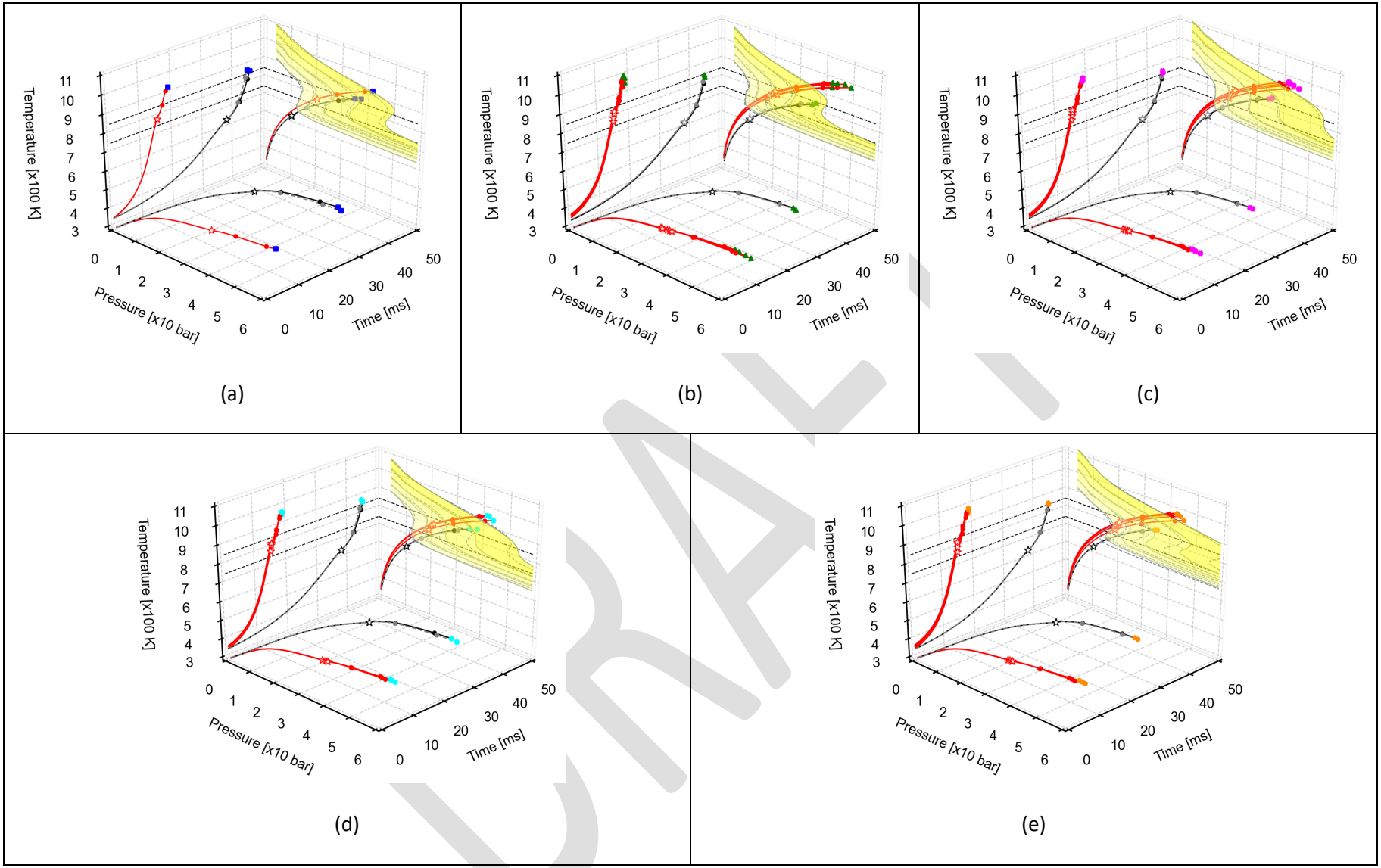

Figure 19: KL-SI P-T-time plot.

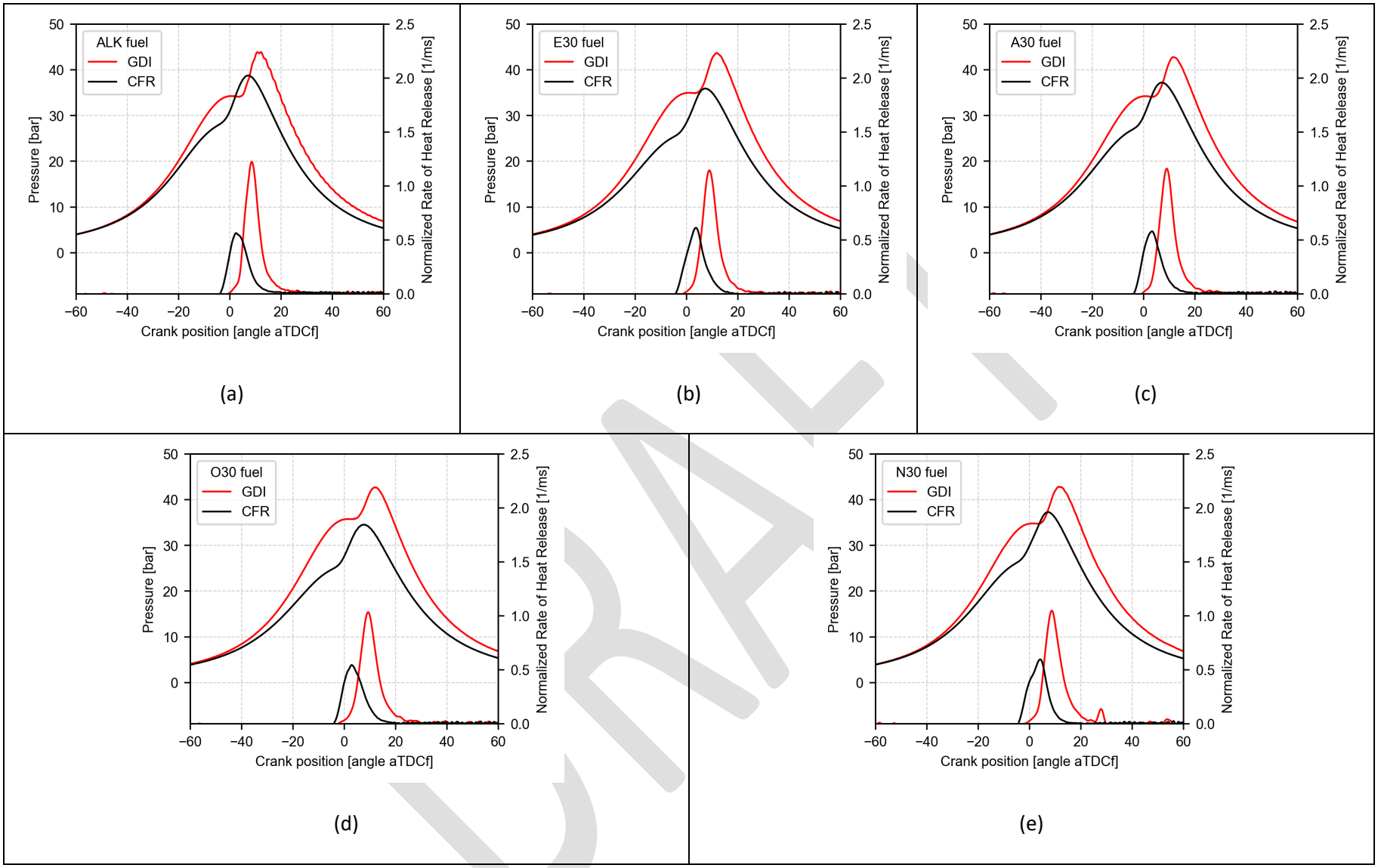

Figure 20: Cylinder pressure and heat release rate characteristics in the GDI engine (red) and the CFR engine (black) under compression ignited low-load operating condition

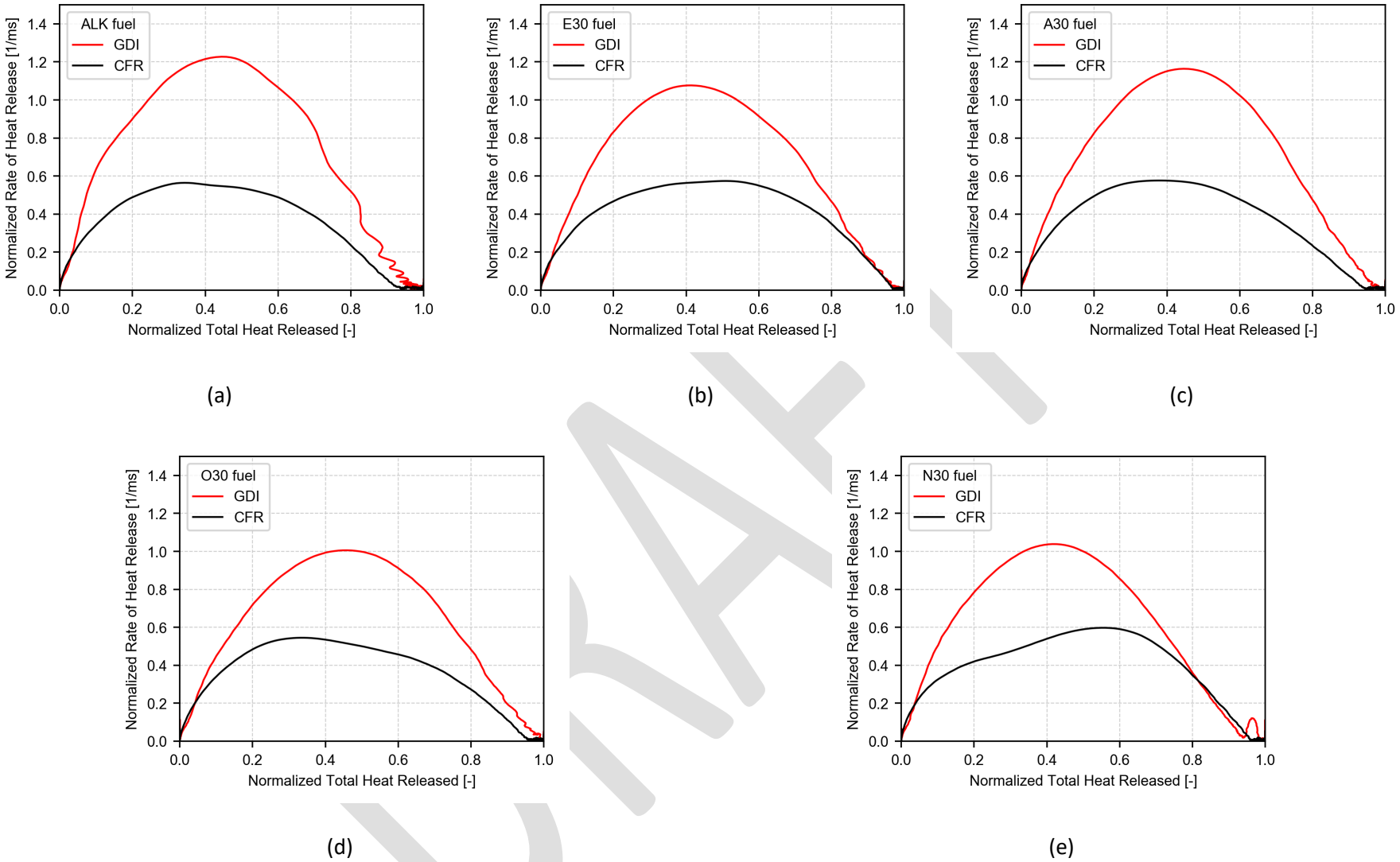

Figure 21: Normalized heat release rate plotted against normalized total heat released for operation in the GDI engine (red) and the CFR engine (black) under low-load compression ignited operation

7 Bibliography

[1] P. M. Najt and D. E. Foster, “Compression-Ignited Homogeneous Charge Combustion,” *SAE Int.*, 1983.

[2] R. Thring, “Homogeneous Charge Compression Ignition (HCCI) Engines,” *SAE Int.*, 1989.

[3] A. Kulzer, J. P. Hathout, C. Sauer, R. Karrelmeyer, W. Fischer, and A. Christ, “Multi-mode combustion strategies with CAI for a GDI engine,” *SAE Tech. Pap.*, vol. 2007, no. 724, 2007.

[4] D. Dahl, I. Denbratt, and L. Koopmans, “An evaluation of different combustion strategies for SI engines in a multi-mode combustion engine,” *SAE Int. J. Engines*, vol. 1, no. 1, pp. 324–335, 2009.

[5] N. Milovanovic, D. Blundell, S. Gedge, and J. Turner, “SI-HCCI-SI mode transition at different engine operating conditions,” *SAE Tech. Pap.*, vol. 2005, no. 724, 2005.

[6] M. Sellnau, W. Moore, J. Sinnamon, K. Hoyer, M. Foster, and H. Husted, “GDCI Multi-Cylinder Engine for High Fuel Efficiency and Low Emissions,” *SAE Int. J. Engines*, vol. 8, no. 2, pp. 2015-01–0834, 2015.

[7] M. Sellnau, M. Foster, W. Moore, J. Sinnamon, K. Hoyer, and W. Klemm, “Second Generation GDCI Multi-Cylinder Engine for High Fuel Efficiency and US Tier 3 Emissions,” *SAE Int. J. Enginess*, vol. 9, no. 2, 2016.

[8] S. Ciatti, M. Johnson, B. Das Adhikary, R. D. Reitz, and A. Knock, "Efficiency and Emissions performance of Multizone Stratified Compression Ignition Using Different Octane Fuels," *SAE Tech. Pap. 2013-01-0263*, no. 2013-01–0263, Apr. 2013.

[9] D. Polovina *et al.*, "Steady-state combustion development of a downsized multi- cylinder engine with range extended HCCI/SACI capability," *SAE Int. J. Engines*, vol. 6, no. 1, pp. 504–519, 2013.

[10] D. Robertson and R. Prucka, "A Review of Spark-Assisted Compression Ignition (SACI) Research in the Context of Realizing Production Control Strategies," *SAE Tech. Pap.*, 2019.

[11] L. Li, H. Xie, T. Chen, W. Yu, and H. Zhao, "Experimental study on spark assisted compression ignition (SACI) combustion with positive valve overlap in a HCCI gasoline engine," *SAE Tech. Pap.*, no. Ci, 2012.

[12] M. Sjöberg and W. Zeng, "Combined Effects of Fuel and Dilution Type on Efficiency Gains of Lean Well-Mixed DISI Engine Operation with Enhanced Ignition and Intake Heating for Enabling Mixed-Mode Combustion," *SAE Int. J. Engines*, vol. 9, no. 2, pp. 750–767, 2016.

[13] Mazda, "MAZDA Next-generation Technology, Press Information," 2017. .

[14] *Standard Test Method for Research Octane Number of Spark-*

Ignition Engine Fuel. USA: ASTM International, 2013.

[15] ASTM Int., "Standard Test Method for Motor Octane Number of Spark-Ignition Engine Fuel 1," *Annu. B. ASTM Stand.*, vol. i, no. C, pp. 1–56, 2011.

[16] G. T. Kalghatgi, "Auto-ignition quality of practical fuels and implications for fuel requirements of future SI and HCCI engines," *SAE Tech. Pap.*, no. 724, 2005.

[17] V. Mittal and J. B. Heywood, "The Relevance of Fuel RON and MON to Knock Onset in Modern SI Engines," vol. 4970, 2008.

[18] G. T. Kalghatgi, "Fuel Anti-Knock Quality - Part I. Engine Studies," *SAE Tech. Pap. Ser.*, vol. 1, no. 724, 2010.

[19] A. Amer *et al.*, "Fuel Effects on Knock in a Highly Boosted Direct Injection Spark Ignition Engine," *SAE Int. J. Fuels Lubr.*, vol. 5, no. 3, pp. 1048–1065, 2012.

[20] T. Davies, R. Cracknell, G. Lovett, L. Cruff, and J. Fowler, "Fuel effects in a boosted DISI engine," in *SAE Technical Papers*, 2011, vol. 2020.

[21] A. D. B. Yates, A. Swarts, and C. L. Viljoen, "Correlating auto-ignition delays and knock-limited spark-advance data for different types of fuel," *SAE Tech. Pap.*, 2005.

[22] A. Prakash *et al.*, "Understanding the Octane Appetite of Modern Vehicles," *SAE Int. J. Fuels Lubr.*, vol. 9, no. 2, pp. 2016-01–0834,

2016.

[23] M. Tao, P. Zhao, J. P. Szybist, P. Lynch, and H. Ge, “Insights into engine autoignition: Combining engine thermodynamic trajectory and fuel ignition delay iso-contour,” *Combust. Flame*, vol. 200, pp. 207–218, 2019.

[24] G. Kalghatgi, K. Morganti, and I. Algunaibet, “Some Insights on the Stochastic Nature of Knock and the Evolution of Hot Spots in the End-Gas during the Engine Cycle from Experimental Measurements of Knock Onset and Knock Intensity,” *SAE Tech. Pap.*, vol. 2017-Octob, no. 1, 2017.

[25] J. C. Peyton Jones, S. Shayestehmanesh, and J. Frey, “A dual-threshold knock controller,” *Int. J. Engine Res.*, vol. 18, no. 8, pp. 837–846, 2017.

[26] A. J. Shahlari and J. B. Ghandhi, “A comparison of engine knock metrics,” *SAE Tech. Pap.*, vol. 4, no. 1, 2012.

[27] G. Kalghatgi, “Knock onset, knock intensity, superknock and preignition in spark ignition engines,” *Int. J. Engine Res.*, vol. 19, no. 1, pp. 7–20, Jan. 2018.

[28] J. M. Spelina, J. C. P. Jones, and J. Frey, “Characterization of knock intensity distributions: Part 1: statistical independence and scalar measures,” *Proc. Inst. Mech. Eng. Part D J. Automob. Eng.*, vol. 228, no. 2, pp. 117–128, 2014.

[29] J. M. Spelina, J. C. P. Jones, and J. Frey, “Characterization of knock intensity distributions: Part 2: parametric models,” *Proc. Inst. Mech. Eng. Part D J. Automob. Eng.*, vol. 227, no. 12, pp. 1650–1660, 2013.

[30] M. Kassa, C. Hall, M. Pamminger, and T. Wallner, “Knock Intensity Distribution and a Stochastic Control Framework for Knock Control,” *J. Dyn. Syst. Meas. Control*, vol. 141, no. 11, pp. 1–9, 2019.

[31] A. Swarts, A. Yates, C. Viljoen, and R. Coetzer, “Standard knock intensity revisited: Atypical burn rate characteristics identified in the CFR octane rating engine,” *SAE Tech. Pap.*, 2004.

[32] A. Swarts, A. Yates, C. Viljoen, and R. Coetzer, “A further study of inconsistencies between autoignition and knock intensity in the CFR octane rating engine,” *SAE Tech. Pap.*, 2005.

[33] A. Swarts and A. Yates, “Insights into the role of autoignition during octane rating,” *SAE Tech. Pap.*, no. 724, 2007.

[34] T. Rockstroh, C. P. Kolodziej, M. C. Jespersen, S. S. Goldsborough, and T. Wallner, “Insights into Engine Knock: Comparison of Knock Metrics across Ranges of Intake Temperature and Pressure in the CFR Engine,” *SAE Int. J. Fuels Lubr.*, vol. 11, no. 4, pp. 545–561, 2018.

[35] J. Pulpeiro Gonzalez, A. Shah, A. Hoth, T. Rockstroh, and C.

Kolodziej, “Statistical analysis of fuel effects on cylinder conditions leading to end-gas autoignition in SI engines,” *SAE Tech. Pap.*, vol. 2019-April, no. April, pp. 1–19, 2019.

[36] A. Swarts, G. L. Anderson, and J. M. Wallace, “Comparing Knock between the CFR Engine and a Single Cylinder Research Engine,” *SAE Tech. Pap. Ser.*, vol. 1, 2019.

[37] V. Arrigoni, G. M. Cornetti, G. Spallanzani, F. Calvi, and A. Tontodonati, “High Speed Knock in S . I . Engines,” 2015.

[38] I. Truedsson, M. Tuner, B. Johansson, and W. Cannella, “Pressure Sensitivity of HCCI Auto-Ignition Temperature for Oxygenated Reference Fuels,” *J. Eng. Gas Turbines Power*, vol. 135, no. 7, p. 072801, 2013.

[39] I. Truedsson, M. Tuner, B. Johansson, and W. Cannella, “Pressure Sensitivity of HCCI Auto-Ignition Temperature for Primary Reference Fuels,” *SAE Int. J. Engines*, vol. 5, no. 3, pp. 1089–1108, Apr. 2012.

[40] V. Kalaskar, D. Kang, and A. L. Boehman, “Impact of Fuel Composition and Intake Pressure on Lean Autoignition of Surrogate Gasoline Fuels in a CFR Engine,” *Energy and Fuels*, vol. 31, no. 10, pp. 11315–11327, 2017.

[41] S. Cheng, Y. Yang, M. J. Brear, D. Kang, S. Bohac, and A. L. Boehman, “Autoignition of pentane isomers in a spark-ignition

engine," vol. 000, pp. 1–8, 2016.

[42] M. U. Waqas, A. Hoth, C. P. Kolodziej, T. Rockstroh, J. P. Gonzalez, and B. Johansson, "Detection of low Temperature heat release (LTHR) in the standard Cooperative Fuel Research (CFR) engine in both SI and HCCI combustion modes," *Fuel*, vol. 256, no. June, p. 115745, 2019.

[43] D. Kang, A. Shah, T. Rockstroh, and S. Goldsborough, "Utilizing Static Autoignition Measurements to Estimate Intake Air Condition Requirements for Compression Ignition in a Multi-Mode Engine - Application of Chemical Kinetic Modeling," in *SAE Technical Papers*, 2019, vol. 2019-April, no. April, pp. 1–15.

[44] A. Hoth, J. Pulpeiro Gonzalez, C. P. Kolodziej, and T. Rockstroh, "Effects of lambda on knocking characteristics and RON rating," *SAE Tech. Pap.*, vol. 2019-April, no. April, pp. 1–14, 2019.

[45] A. Hoth, C. P. Kolodziej, T. Rockstroh, and T. Wallner, "Combustion Characteristics of PRF and TSF Ethanol Blends with RON 98 in an Instrumented CFR Engine," *SAE Tech. Pap.*, vol. 2018-Septe, pp. 1–14, 2018.

[46] R. L. McCormick *et al.*, "Co-Optimization of Fuels & Engines: Properties of Co-Optima Core Research Gasolines," Golden, CO (United States), Aug. 2018.

[47] M. J. McNenly, R. A. Whitesides, and D. L. Flowers, "Faster solvers

for large kinetic mechanisms using adaptive preconditioners," *Proc. Combust. Inst.*, vol. 35, no. 1, pp. 581–587, 2015.

[48] M. Mehl *et al.*, "A Comprehensive Detailed Kinetic Mechanism for the Simulation of Transportation Fuels," in *10th U.S. National Combustion Meeting*, 2017.

[49] Y. Li, C. W. Zhou, K. P. Somers, K. Zhang, and H. J. Curran, "The oxidation of 2-butene: A high pressure ignition delay, kinetic modeling study and reactivity comparison with isobutene and 1-butene," *Proc. Combust. Inst.*, vol. 36, no. 1, pp. 403–411, 2017.

[50] J. Bugler *et al.*, "An ignition delay time and chemical kinetic modeling study of the pentane isomers," *Combust. Flame*, vol. 163, pp. 138–156, 2016.

[51] K. Zhang, C. Banyon, C. Togbé, P. Dagaut, J. Bugler, and H. J. Curran, "An experimental and kinetic modeling study of n-hexane oxidation," *Combust. Flame*, vol. 162, no. 11, pp. 4194–4207, 2015.

[52] K. Zhang *et al.*, "An updated experimental and kinetic modeling study of n-heptane oxidation," *Combust. Flame*, vol. 172, pp. 116–135, 2016.

[53] N. Atef *et al.*, "A comprehensive iso-octane combustion model with improved thermochemistry and chemical kinetics," *Combust. Flame*, vol. 178, pp. 111–134, 2017.

[54] Y. Zhang, Y. Pei, M. Tang, and M. Traver, “Injector Spray Pattern Effects on Gasoline Compression Ignition in a Heavy-Duty Diesel Engine,” pp. 1–11, 2019.

[55] Y. Zhang, K. P. Somers, M. Mehl, W. J. Pitz, R. F. Cracknell, and H. J. Curran, “Probing the antagonistic effect of toluene as a component in surrogate fuel models at low temperatures and high pressures. A case study of toluene/dimethyl ether mixtures,” *Proc. Combust. Inst.*, vol. 36, no. 1, pp. 413–421, 2017.

[56] G. Kukkadapu *et al.*, “Kinetic modeling study of surrogate components for gasoline, jet and diesel fuels: C7-C11 methylated aromatics,” *Proc. Combust. Inst.*, vol. 37, no. 1, pp. 521–529, 2019.

[57] S. W. Wagnon *et al.*, “Experimental and modeling studies of a biofuel surrogate compound: laminar burning velocities and jet-stirred reactor measurements of anisole,” *Combust. Flame*, vol. 189, pp. 325–336, 2018.

[58] M. J. Al Rashidi *et al.*, “Cyclopentane combustion. Part II. Ignition delay measurements and mechanism validation,” *Combust. Flame*, vol. 183, pp. 372–385, 2017.

[59] M. J. Al Rashidi, M. Mehl, W. J. Pitz, S. Mohamed, and S. M. Sarathy, “Cyclopentane combustion chemistry. Part I: Mechanism development and computational kinetics,” *Combust. Flame*, vol. 183, pp. 358–371, 2017.

[60] M. J. Al Rashidi *et al.*, "Elucidating reactivity regimes in cyclopentane oxidation: Jet stirred reactor experiments, computational chemistry, and kinetic modeling," *Proc. Combust. Inst.*, vol. 36, no. 1, pp. 469–477, 2017.

[61] Y. Zhang, H. El-Merhubi, B. Lefort, L. Le Moyne, H. J. Curran, and A. Kéromnès, "Probing the low-temperature chemistry of ethanol via the addition of dimethyl ether," *Combust. Flame*, vol. 190, pp. 74–86, 2018.

[62] P. Risberg, D. Johansson, J. Andrae, G. Kalghatgi, P. Björnbom, and H.-E. Ångström, "The Influence of NO on the Combustion Phasing in an HCCI Engine," in *SAE Technical Papers*, 2006, vol. 2006, no. 724.

[63] M. Sjöberg, D. Vuilleumier, N. Kim, N. Yokoo, T. Tomoda, and K. Nakata, "On the Role of Nitric Oxide for the Knock-Mitigation Effectiveness of EGR in a DISI Engine Operated with Various Gasoline Fuels," *SAE Tech. Pap. Ser.*, vol. 1, no. 2, 2019.

[64] Z. Chen, H. Yuan, T. M. Foong, Y. Yang, and M. Brear, "The impact of nitric oxide on knock in the octane rating engine," *Fuel*, vol. 235, no. August 2018, pp. 495–503, Jan. 2019.

[65] Z. Chen, P. Zhang, Y. Yang, M. J. Brear, X. He, and Z. Wang, "Impact of nitric oxide (NO) on n-heptane autoignition in a rapid compression machine," *Combust. Flame*, vol. 186, pp. 94–104, 2017.

[66] S. Cheng, Y. Yang, M. J. Brear, D. Kang, S. Bohac, and A. L. Boehman, “Autoignition of pentane isomers in a spark-ignition engine,” *Proc. Combust. Inst.*, vol. 36, no. 3, pp. 3499–3506, 2017.

[67] J. W. Fox, W. K. Cheng, and J. B. Heywood, “A Model for Predicting Residual Gas Fraction in Spark-Ignition Engines,” *SAE Int.*, no. 412, 1993.

[68] E. Bartholomew, “NEW KNOCK-TESTING METHODS NEEDED TO MATCH ENGINE AND FUEL PROGRESS,” in *Pre-1964 SAE Technical Papers*, 1961.

[69] J. P. Szybist and D. A. Splitter, “Impact of Engine Pressure-Temperature Trajectory on Autoignition for Varying Fuel Properties,” *Appl. Energy Combust. Sci.*, vol. 1–4, no. June, p. 100003, 2020.

[70] M. A. Ratcliff, J. Burton, P. Sindler, E. Christensen, L. Fouts, and R. L. McCormick, “Effects of Heat of Vaporization and Octane Sensitivity on Knock-Limited Spark Ignition Engine Performance,” *SAE Tech. Pap. Ser.*, vol. 1, pp. 1–14, 2018.

[71] Y. Song, Y. He, Y. Yu, B. Moreau, and F. Foucher, “E ff ect of Exhaust Gas Recirculation and NO on Ignition Delay Times of Iso-octane in a Rapid Compression Machine,” 2020.

[72] M. U. Waqas, A. Hoth, C. P. Kolodziej, T. Rockstroh, J. P. Gonzalez, and B. Johansson, “Characterization of Low Temperature

Reactions in the Standard Cooperative Fuel Research (CFR) Engine," *SAE Int. J. Engines*, vol. 12, no. 5, pp. 597–610, 2019.

[73] T. Rockstroh, A. Fridlyand, S. Ciatti, W. Cannella, and S. S. Goldsborough, "Autoignition behavior of a full boiling-range gasoline: Observations in RCM and GCI engine environments," *Combust. Flame*, vol. 209, pp. 239–255, Nov. 2019.

[74] S. M. Sarathy *et al.*, "Three-stage heat release in n-heptane auto-ignition," *Proc. Combust. Inst.*, vol. 000, pp. 1–8, 2018.

[75] T. Rockstroh, G. Floweday, and A. Yates, "Optimisation of synthetic gasoline blend recipes for use in modern charge boosted GDI engines," *Fuel*, vol. 186, pp. 800–820, 2016.

[76] R. Cracknell *et al.*, "Is the 'k Value' of an Engine Truly Fuel Independent?," *SAE Tech. Pap.*, vol. 2020-April, no. April, pp. 1–10, 2020.

Appendix A Test fuel properties

Property	Method	ALK	E30	A30	O30	N30
LHV[a]	D4809	44.52	38.17	42.95	44.07	43.21
Distillation	ASTM D86 [°C]					
10%		93.1	60.7	59.4	77.1	55.7
50%		100.3	74.3	108.1	104.3	87.4
90%		105.9	155.2	157.9	136.2	142.7
Composition Information						
Aromatic	ASTM D6729 (wt%)	1	16.1	45.8	15	38.4
Olefin		0.1	5.2	4.1	32.1	1.5
Total saturates		98.5	43.8	48.5	52.1	59.6
n-paraffins		2.5	11.1	6.7	9.6	6.9
i-paraffins		96	25.5	33.9	39.6	28.7
Cycloalkanes		0	7.2	7.9	2.9	24
Unidentified		0.4	2.9	1.6	0.8	0.5
Oxygenates		0	32	0	0	0
Carbon	ASTM D5291 (wt%)	83.75	74.78	87.22	85.40	87.08
Hydrogen		15.80	13.79	13.12	14.50	13.24

[a]LHV – Lower Heating Value [MJ/kg]